RSC Advances

This is an *Accepted Manuscript*, which has been through the Royal Society of Chemistry peer review process and has been accepted for publication.

Accepted Manuscripts are published online shortly after acceptance, before technical editing, formatting and proof reading. Using this free service, authors can make their results available to the community, in citable form, before we publish the edited article. This *Accepted Manuscript* will be replaced by the edited, formatted and paginated article as soon as this is available.

You can find more information about *Accepted Manuscripts* in the Information for Authors.

Please note that technical editing may introduce minor changes to the text and/or graphics, which may alter content. The journal's standard Terms & Conditions and the Ethical guidelines still apply. In no event shall the Royal Society of Chemistry be held responsible for any errors or omissions in this *Accepted Manuscript* or any consequences arising from the use of any information it contains.

ROYAL SOCIETY OF CHEMISTRY

www.rsc.org/advances

Please do not adjust margins

Journal Name

ARTICLE

A label-free electrochemical immunosensor for carcinoembryonic antigen detection at graphene doped with poly(3,4-ethylenedioxythiophene)/Au nanoparticles platform

Received 00th January 20xx,

Accepted 00th January 20xx

DOI: 10.1039/x0xx00000x

www.rsc.org/

Yan-Sha Gao,[a,b] Jing-Kun Xu,[b*] Li-Min Lu,[a*] Xiao-Fei Zhu,[b] Wen-Min Wang,[a] Tao-Tao Yang,[b] Kai-Xin Zhang,[b] Yong-Fang Yu[a]

In this work, a two-step method was developed for the fabrication of graphene doped poly(3,4-ethylenedioxythiophene)/Au nanoparticles (AuNPs/PEDOT/GR) sensing platform. PEDOT nanorods grown on graphene oxide nanosheets (PEDOT/GO) were firstly synthesized by liquid-liquid interfacial polymerization, followed by the chemical reduction of $HAuCl_4$ by $NaBH_4$. During the reduction process, GO doped in the PEDOT was also reduced to a more conductive form of GR. The obtained AuNPs/PEDOT/GR showed excellent conductivity and large surface area. Thus, a simple and sensitive label-free immunosensor based on AuNPs/PEDOT/GR nanocomposite has been proposed to detect carcinoembryonic antigen (CEA) by measuring the change of electrochemical response before and after the immunoreaction. Under the optimized conditions, the linear range of the proposed immunosensor is estimated to be from 0.0004 to 40 ng mL^{-1} (R^2 = 0.9969) and the detection limit is estimated to be 0.1 pg mL^{-1} at a signal-to-noise ratio of 3, respectively. Moreover, the immunosensor was examined for use in the determination of CEA in real human serum samples with satisfactory results.

Introduction

Tumor markers are useful tools in the diagnosis of tumors, whose measurement or identification is of great importance for patient diagnosis or clinical management. Carcinoembryonic antigen (CEA), a tumor-associated antigen with a molecular weight of approximately 200 kDa, is a glycoprotein involved in cell adhesion, and is a glycosyl phosphatidyl inositol cell surface anchored glycoprotein.[1-4] Basically, the low levels of CEA in colon tissue of adults are reported as 2.5-5.0 μg L^{-1}.[5] However, an elevated CEA concentration in adult plasma is widely accepted as an early indicator for diagnosis and prognostics of some cancerous diseases such as breast tumors, colon tumors, ovarian carcinoma and cervical carcinomas.[6-9] Hence, it is very important to detect trace amount of CEA for early discovery, early diagnosis and early treatment. Immunosensors, particularly the electrochemical immunosensors, have been proved to be ideal methods for the detection of CEA because of their high accuracy, sensitivity and selectivity, low cost and easy operation.[10-11] Depending on whether labels are used or not, immunosensors are divided into two categories: labeled type and label-free type. In general, most of the labeled immunosensors must use specific material as the second antibody's marker.[9,43] However, the activity of the prepared conjugates must be carefully controlled, and some additional reagents and procedures must be involved. Faced with this dilemma, label-free immunosensor especially has attracted great research interests due to its simple preparation, more cost effectiveness and well activity conservation of antibodies or antigens.

For an electrochemical immunosensor, its performance is critically dependent on the properties of electrode interface. Recently, great interest in the preparation of nanocomposites of conducting polymers and graphene or graphene derivatives has increased dramatically due to their synergistic effects.[12-14] Among the conducting polymers, poly(3,4-ethylenedioxythiophene) (PEDOT) is the most investigated conducting polymer due to its excellent electrochemical activity, high electric conductivity, low bandgap, excellent environmental stability, and transparency in the doped state.[15-16] Moreover, PEDOT nanostructures including nanorods and nanotubes are deemed as excellent sensing materials[17-18] because of their high surface area and capability of offering amplified sensitivity. Template method is often used as a universal and powerful controlled approach towards obtaining nanostructures. Recently, graphene oxide (GO), the oxygenated derivative of graphene (GR), bearing epoxy, hydroxyl, carbonyl, and carboxyl groups on the single atomic layer of carbon, is unique and much more promising than other

[a] College of Science, Jiangxi Agricultural University, Nanchang 330045, PR China
[b] Jiangxi Key Laboratory of Organic Chemistry, Jiangxi Science and Technology Normal University, Nanchang 330013, PR China
*To whom correspondence should be addressed.
E-mail: xujingkun@tsinghua.org.cn (J. Xu), lulimin816@hotmail.com.
Tel.: +86 791 8537967; Fax: +86 791 3823320

RSC Advances Accepted Manuscript

Please do not adjust margins

carbon materials like carbon nanotubes carbon fibers and fullerenes.[19-22] The outstanding structural, mechanical and thermal properties and large surface area of GO offer the possibility of it being an excellent filler or template for fabricating nanocomposites.[23] Thus, nano-hybrid composites of PEDOT/GO can be prepared by a simple liquid-liquid interfacial polymerization process due to its unique advantages of simple synthesis and purification without template moving steps.[24]

Au nanoparticles (AuNPs), one of electroactive noble materials, have been widely used in the fabrication of electrochemical immunosensor because of advantages such as good conductivity and biocompatibility, easy and rapid synthesis, narrow size distribution and excellent stability.[25] They can provide more active sites for the binding of antibodies and can accelerate the electron transfer process for signal amplification to achieve high sensitivity.[26] In order to further improve the conductivity and increase the surface-to-volume ratio, Au nanoparticles should be loaded onto some nano-matrixs prior to the fabrication of electrochemical immunosensor.

In this work, we described a new electrochemical immunosensor for the detection of CEA based on AuNPs/PEDOT/GR composite for the first time. For the preparation of AuNPs/PEDOT/GR composite, PEDOT/GO composite was firstly synthesized by a simple liquid-liquid interfacial polymerization according to our previous work.[27] And then a mixture of the obtained PEDOT/GO and $HAuCl_4$ were reduced by $NaBH_4$ at room temperature. In this chemical reduction process, GO and $HAuCl_4$ were reduced to GR and AuNPs, respectively. The prominent biocompatibility, excellent electron transport capability and large specific surface area of AuNPs/PEDOT/GR can greatly enhance the electrical signal and improve the immobilizing amount of antibody on the electrode surface. The sensitive detection of CEA was realized by monitoring the change in the electrode response of $[Fe(CN)_6]^{3-/4-}$ before and after the antigen-antibody reaction. The fabricated immunosensor exhibited a good response for the detection of CEA and showed great potential for application in real sample analysis.

2 Experimental

2.1 Chemicals

CEA and anti-CEA antibody were purchased from Bosai Biotechnology co., ltd. Human serum samples were purchased from a local hospital. Bovine serum albumin (BSA) and 3,4-ethylenedioxythiophene (EDOT) was purchased from Sigma-Aldrich. Graphene oxide (GO) was obtained from Nanjing Xianfeng nano Co. The diameter of the GO was about 1~5 nm, and the thickness was about 0.8~1.2 nm. $HAuCl_4 \cdot 3H_2O$ was purchased from Sinopharm Chem. Re. Co. Ltd. Ferric chloride ($FeCl_3$) and chloroform ($CHCl_3$) were purchased from Shanghai Chemical Co., Ltd., (Shanghai, China). Phosphate buffer (0.1 M, pH 7.0) was used as an electrolyte for all electrochemistry measurement. All other reagents were of analytical grade and were used without further purification and double distilled water was used throughout the experiments.

2.2 Apparatus

Scanning electron microscopy (SEM) analysis was performed using a Hitachi S-3000 N scanning electron microscope. Transmission electron microscope (TEM) images were obtained at a FEI Tecnai G20 transmission electron microscope (FEI Co., Ltd., America). X-ray diffraction (XRD) patterns were recorded on a Rigaku powder diffractometer equipped with Cu Kα 1 radiation (λ = 1.5406 Å). A Raman spectrum (Bruker Raman RM2000) was used to analyze the samples using a 785 nm laser. Infrared spectra was recorded using Bruker Vertex 70 Fourier spectrometer with samples in KBr pellets. The cyclic voltammetric and electrochemical impedance spectroscopy measurements were carried out on a CHI660D electrochemical workstation (Shanghai, China). A standard three-electrode cell contained a platinum wire auxiliary electrode, a saturated calomel reference electrode (SCE) and the modified glassy carbon electrode (GCE) (Φ = 3 mm) as working electrode were employed for electrochemical studies. All potential values given below refer to SCE.

2.3 Preparation of PEDOT/GO and AuNPs/PEDOT/GR nanocomposites

A typical procedure for the synthesis of PEDOT/GO composites was shown in Scheme 1. 1 mL of $FeCl_3$ (1 M) was added into 1 mL of GO dispersion aqueous (0.5 mg mL^{-1}), followed by sonication for 10 min. Then the above solution was slowly added into 2 mL of EDOT solution in $CHCl_3$ (25 mg mL^{-1}) and an interface was generated between two layers. The above mixture was heated at 50 °C under static conditions. After the reaction proceed for 24 h, the upper layer mixture was centrifuged, and the precipitae was washed with distilled water and ethanol several times, respectively. The resulting precipitates were collected for further use.

In the second step, the above-obtained PEDOT/GO precipitates were dispersed in deionized water under sonication. Prior to AuNPs loading, all glasswares were soaked in a mixture of nitric acid and hydrochloric acid (1:3) for 1 h, and then thoroughly washed with deionized water. 1 mL $HAuCl_4 \cdot 3H_2O$ (5 mM) aqueous solution was added to the above-prepared PEDOT/GO suspension (8 mL), and the mixture was vigorously stirred. 15 min later, an aqueous solution of $NaBH_4$ (0.1 M) was added and stirring continued for the other 6 h at room temperature. In this chemical reduction process, both GO and Au ions are reduced completely. Then the resulting nanocomposites of AuNPs/PEDOT/GR were collected, washed and re-dispersed in 1 mL water and stored in 4 ºC for further use.

2.4 The preparation of immunosensor

The glassy carbon electrode (GCE) was mechanically polished with chamois leather containing 0.05 μm alumina slurry, and then it was ultrasonically cleaned with doubly distilled water, absolute ethanol and doubly distilled water each for 5 min, respectively. 5 μL of the AuNPs/PEDOT/GR suspension was transferred on the surface of GCE and then dried in air.

The obtained above modified electrode AuNPs/PEDOT/GR/GCE was incubated in anti-CEA antibody solution (20 μg mL^{-1}) to immobilize antibody molecules onto the surface of AuNPs. After washing, 5 μL of 1 wt% BSA solution was added and incubated for 30 min to eliminate nonspecific binding sites. Subsequently, the electrode was washed and incubated with a varying concentration of CEA for 50 min at room temperature, and then the electrode was washed extensively to remove unbounded CEA molecules. The prepared electrode was ready for measurement after washing and the fabricated procedure of the immunosensor was shown in scheme 1.

RSC Advances Accepted Manuscript

This journal is © The Royal Society of Chemistry 20xx

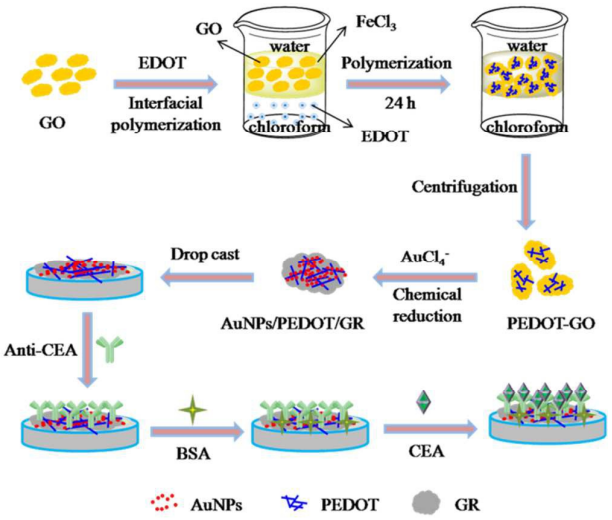

Scheme 1 Schematic illustration of the fabrication procedure of the immunosensor.

2.5 Experimental measurements

Electrochemical experiments were carried out in 5 mL phosphate buffer (pH 7.0) containing 5 mM $[Fe(CN)_6]^{3-/4-}$ at room temperature. Cyclic voltammetry experiments were recorded at a potential range from - 0.2 to 0.6 V (*vs*. SCE) with scan rate of 50 mV s^{-1}. Differential pulse voltammetry (DPV) was recorded at a potential from - 0.2 to 0.6 V (*vs*. SCE) with a pulse period of 0.2 s and amplitude of 50 mV. Electrochemical impedance spectroscopy (EIS) was recorded within a frequency range from 0.1 Hz to 100 kHz, and amplitude of 5 mV.

3 Results and discussion

3.1. Characterization

The surface morphology of as-prepared PEDOT/GO (A) and AuNPs/PEDOT/GR (B and C) films were investigated by SEM. As for the PEDOT/GO (Fig. 1A) composite, it can be seen that the GO sheets had been decorated randomly with a large amount of PEDOT nanorods. It is also found that the structure of PEODT/GO composite prepared by interface polymerization method is the same as it was in previous literatures.[28-29] Therefore, it is reasonable to believe that the carboxyl, hydroxyl and epoxide, and these randomly distributed functional groups on the surface and edges of GO sheets served act as nucleation sites for growth of the nanorods-like PEDOT.[30-31] As the nanorods-like PEDOT structures give a high specific surface area compared to their conventional bulk counterparts,[24] it can act as matrix carriers to anchor a large amount of AuNPs. From the Fig. 1B and C, it can be observed that a much higher density of AuNPs with smaller sizes were formed on the PEDOT nanorods.

In order to further confirm the components, the AuNPs/PEDOT/GR composite of energy dispersive spectrum (EDS) analysis was performed. The EDS profile in Figure 1D revealed the presence of Au, C, O and S, the component elements of the composite of AuNPs/PEDOT/GR. Cl and Fe came from the oxidants and In, Si and Ca came from the ITO glasses.

For clear characterization of the products, the TEM of PEDOT/GO (A) and AuNPs/PEDOT/GR (B) were presented in Fig. 2. As can be seen in Fig. 2A, it was obvious that the GO sheets had been decorated randomly with the PEDOT nanorods, which illustrated the successful combination with PEDOT and GO. As for AuNPs/PEDOT/GR (Fig. 2B), the composite of PEDOT-GR are decorated successfully with many well-dispersed AuNPs. It is noted that the particle size of the Au distributed with an average diameter of about (10±2) nm. In fact, this was just an advantage over the composite surface for increasing the immobilized amount of anti-CEA antibody.[32]

The FT-IR spectras of PEDOT/GO (a) and AuNPs/PEDOT/GR (b) were shown in Fig. 3A. In the spectrum of the PEDOT/GO (a), a typical peak at 1732 cm^{-1} attributed to the C=O stretching was observed, suggesting the existence of oxygen functionalities at GO surface. The spectrum of PEDOT/GO also showed bands originating from OH stretching and absorbed water (3380 cm^{-1}), C=C (1631 cm^{-1}), C–C (1404 cm^{-1}), and C–O–C (1094 cm^{-1}). There were other adsorption peaks at 821 and 685 cm^{-1}, which corresponded to vibration modes of C–S–C bond of thiophene ring,[33] suggesting the PEDOT has been successfully decorated on the surface of the GO sheets. In comparison with the PEDOT/GO, besides the same peaks derived from PEDOT/GO, the absorption peaks appeared at 1731 and 1094 cm^{-1} weakened dramatically in the FTIR spectra of AuNPs/PEDOT/GR (b), which indicated that the GO was effectively transformed into GR in the process of synthesis.

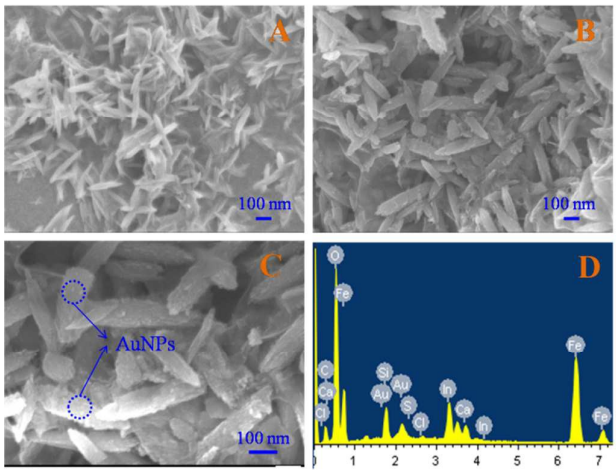

Fig. 1. SEM image of PEDOT/GO (A), AuNPs/PEDOT/GR (B) and magnification SEM image of AuNPs/PEDOT/GR (C) films; EDS elemental analysis of AuNPs/PEDOT/GR (D).

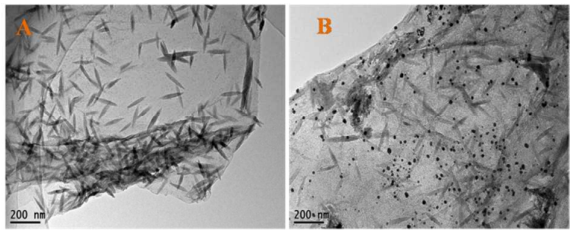

Fig. 2. TEM images of PEDOT/GO (A) and AuNPs/PEDOT/GR (B) nanocomposites.

RSC Advances Accepted Manuscript

Raman spectroscopy was further used to evaluate the nature and the relative quantities of carbonaceous materials, formed on the particle surfaces in the as-prepared composites.[34] Fig. 3B shows the Raman spectra of PEDOT/GO (a) and AuNPs/PEDOT/GR (b), which were very similar to the previous reports.[18] For PEDOT/GO and AuNPs/PEDOT/GR composites, the characteristic peaks at 440, 574 and 1101 cm^{-1} were assigned with C–O–C bond deformation. Vibrational modes observed at 853 and 986 cm^{-1} were assigned to O–C–C deformation and oxyethylene ring deformation. The appearance of peaks at 1253 and 1363 cm^{-1} were due to the thiophene C–C inter-ring stretching. The peaks at 1424 and 1506 cm^{-1} were corresponded to symmetric and antisymmetric C=C stretching, respectively.[35] Moreover, a band of PEDOT/GO at 1563 cm^{-1} shifted to 1550 cm^{-1} in AuNPs/PEDOT/GR, which might be due to the fact that GO in the nanocomposite was reduced to GR.[36]

The structure of the PEDOT/GO (a) and AuNPs/PEDOT/GR (b) were investigated by XRD and the pattern was shown in Fig. 4. For the patterns of PEDOT/GO (a), the peak at about 11.9° could be clearly observed, while it was disappeared in the pattern of the AuNPs/PEDOT/GR (b). The disappearance of the peak at about 11.9° confirmed that most oxygen functional groups were removed and GO was reduced to GR successfully.[37-38] Besides, the PEDOT/GO displayed a broad diffraction peak at 2θ = 26.96°, which can be attributed to the intermolecular spacing of polymer backbone or assigned to the (020) reflection.[39] Furthermore, XRD analysis of AuNPs/PEDOT/GR (b) also confirmed the diffraction features appearing at 2θ as 38.35°, 44.57°, 64.78°, 77.89° and 81.97° that correspond to the (111), (200), (220), (311) and (222) planes of the standard cubic phase of Au, respectively.[40]

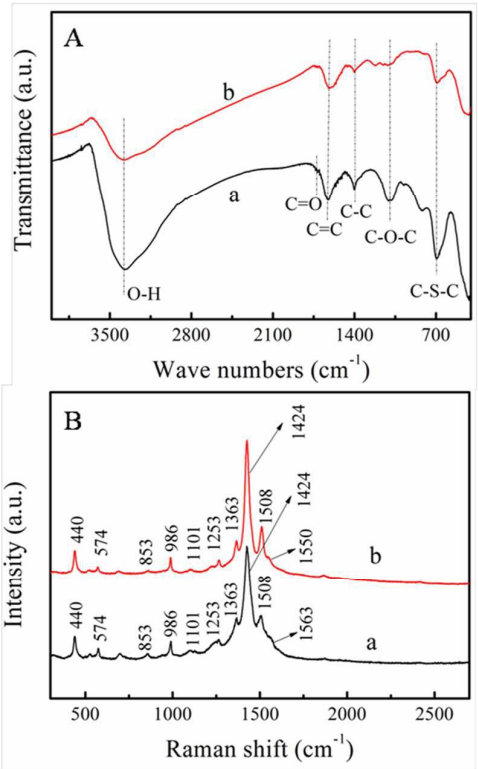

Fig. 3. (A) FT-IR and (B) Raman spectroscopy of PEDOT/GO (a) and AuNPs/PEDOT/GR (b) nanocomposites.

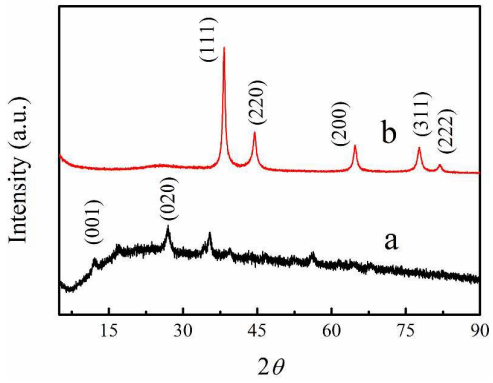

Fig. 4. XRD patterns of PEDOT/GO (a) and AuNPs/PEDOT/GR (b) nanocomposites.

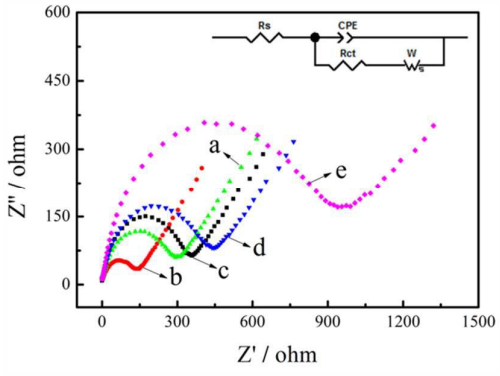

Fig. 5. EIS of bare GCE (a), PEDOT/GO (b), AuNPs/PEDOT/GR (c), Ab/AuNPs/PEDOT/GR/GCE (d), BSA/Ab/AuNPs/ PEDOT/GR/GCE (e) and BSA/Ab/AuNPs/ PEDOT/GR/GCE after incubated with 4 ng mL^{-1} of CEA (f) in 5.0 mM $K_3Fe(CN)_6/K_4Fe(CN)_6$ (1:1) containing 0.1 M KCl. Inset: equivalent circuit for fitting the plots. Rs: solution resistance; Rct: chargetransfer resistance; CPE: constant phase element, which is a complex of various elements; W: Warburg resistance, which reflects diffusion barrier in the low frequency part.

3.2 Electrochemical characteristics of the immunosensor

Electrochemical impedance spectroscopy (EIS) is an effective tool for monitoring the interfacial properties of surface-modified electrodes. In the study, the impedance changes of the immunosensor surface in the fabrication process and the formation of an antigen–antibody complex were observed by EIS (Fig. 5). The data can be fitted with a modified Randles equivalent circuit (inset in Fig. 5).[41] Fig. 3 presents the representative impedance spectrum of the bare GCE (a), PEDOT/GO (b), AuNPs/PEDOT/GR (c), Ab/AuNPs/PEDOT/GR/GCE (d), BSA/Ab/AuNPs/PEDOT/GR/GCE (e) and BSA/Ab/AuNPs/PEDOT/GR/GCE after incubated with 4 ng mL^{-1} of CEA (f) in 5.0 mM $K_3Fe(CN)_6/K_4Fe(CN)_6$ (1:1) containing 0.1 M KCl. After the PEDOT/GO was modified onto the GCE (b), the semicircle dramatically decreased relative to the bare GCE (a) owing to the good conductivity of PEDOT nanorods. Compared with PEDOT/GO (b), the semicircle of AuNPs/PEDOT/GR (c) decreased distinctively, suggesting faster electron transfer

RSC Advances Accepted Manuscript

This journal is © The Royal Society of Chemistry 20xx

kinetics of $[Fe(CN)_6]^{3-/4-}$ on the electrode surface, which was ascribed to the significantly improved electrical conductivity of PEDOT and GR. When anti-CEA was immobilized onto the modified electrode, the Ret presented an apparent increase (d), which might be due to the fact that the anti-CEA was successfully immobilized on the surface and formed an additional barrier and blocked the electron exchange between the redox probe and the electrode. The Ret increased in a similar way after BSA was used to block nonspecific sites (e). After the immunosensor was incubated with the CEA antigen, the Ret further increased (f), which indicated the formation of a hydrophobic immunocomplex layer hindering the electron transfer.

Cyclic voltammetry (CV) was employed to monitor each immobilization step and the corresponding results were shown in Fig. 6A. The redox-labeled $[Fe(CN)_6]^{3-/4-}$ revealed a reversible CV at the bare GCE (a). After the pretreated GCE was modified with AuNPs/PEDOT/GR, the peak current increased (b), implying that the AuNPs/PEDOT/GR nanocomposites facilitated the electron transfer. However, the peak current decreased after anti-CEA was immobilized onto the modified electrode surface (c), which indicated that the big protein molecules blocked the electron transfer, in agreement with the results of EIS. A further decrease of the peak current was observed when BSA was employed to block non-specific sites (d). After the immunosensor was incubated with CEA antigen, the peak current decreased due to the immunocomplex retarding the electron transfer (e).

Useful information involving electrochemical mechanism usually can be acquired from the relationship between peak current and scan rate. The CV of the proposed immunosensor in 5.0 mM $[Fe(CN)_6]^{3-/4-}$ solution at different scan rates are investigated in the range of 10-250 mV s^{-1}. It is clearly observed that the potentials and peak currents are dependent on the scan rate in Fig. 6B. As shown in the inset of Fig. 6B, both the anodic and cathodic peak currents were directly proportional to the square root of scan rate, suggesting a diffusion controlled process.

3.3. Optimization of experimental conditions

The factors influencing the performance of the immunosensor included the buffer pH, the incubation temperature, and the incubation time. The effect of pH on the detection solution on the immunosensor behavior was investigated over a pH range from 5.5 to 8.0 with 0.4 ng mL^{-1} CEA. As shown in Fig. 7A, the current responses increased from pH 5.5 to 7.0 to reach the maximum value and decreased from pH 7.0 to 8.0. Hence, pH 7.0 was chosen as the optimum pH of the detection solution throughout this study to obtain a high sensitivity.

Incubation time is another important parameter in the construction of the immunosensor. As shown in Fig. 7B, the immunosensor was incubated in a constant concentration of CEA for different times. Δ I rapidly increased within the first 50 min and then decreased. Therefore, 50 min was chosen as the optimal incubation time.

The effect of temperature on the current responses was also studied at the temperature range from 10 to 50 °C. As shown in Fig. 7C, maximum response was achieved at a temperature around 35 °C. However, temperature above 40 °C might cause irreversible denaturation of CEA and anti-CEA. As is well known, long-time use in high temperature may damage the modifier and affect the lifetime of the immunosensor. Thus, 35 °C was the best incubation temperature to take immunoreaction.

3.4 Analytical performance of immunosensor

To assess the sensitivity and dynamic working range of the electrochemical immunosensor, a differential pulse voltammetry (DPV) measurement was applied to detect CEA standards in pH 7.0 phosphate buffer containing 5.0 mM $Fe(CN)_6^{3-/4-}$ solution. As can be seen in Fig. 8A, when the CEA concentration increased, the DPV current signal decreased accordingly. The reason can be attributed to the insulating CEA protein layer acting as a nonconductor obstructed the electron transfer between the electrolyte and electrode surface.[42] Therefore, it can be seen that the DPV response of the immunosensor decreased with the increment of CEA concentrations, and exhibited a good linear relationship with the logarithm of CEA concentration from 0.0004 to 40 ng mL^{-1} (Fig. 8B). The linear regression equation was adjusted to ΔI (μA) = 0.4696 + 0.1165 × log *C* [CEA] (ng mL^{-1}, R^2 = 0.9969). The relative standard deviations (RSD) for the measurement of each data point were less than 5.0%. The limit of detection (LOD) was 0.1 pg mL^{-1} at a signal-to-noise ratio of 3.

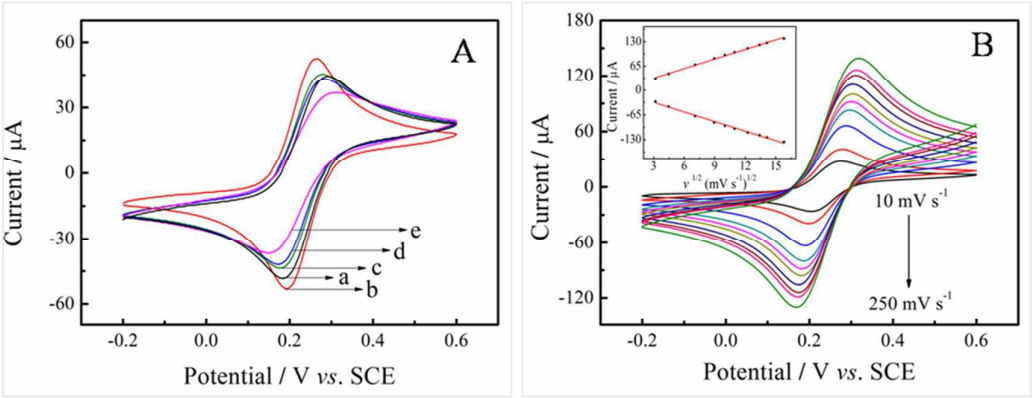

Fig. 6. (A) CV of bare GCE (a), AuNPs/PEDOT/GR (b), Ab/AuNPs/PEDOT/GR/GCE (c), BSA/Ab/AuNPs/PEDOT/GR/GCE (d) and BSA/Ab/AuNPs/PEDOT/GR/GCE after incubated with 4 ng mL^{-1} of CEA (e) in 5.0 mM $K_3Fe(CN)_6/K_4Fe(CN)_6$ (1:1) containing 0.1 M KCl. (B) CVs of the modified electrodes at different scan rates (from inner to outer): 10, 20, 50, 80, 120, 150, 180, 200 and 250 mV s^{-1}; The inset shows the dependence of redox peak currents on the square root of scan rates.

RSC Advances Accepted Manuscript

Journal Name

ARTICLE

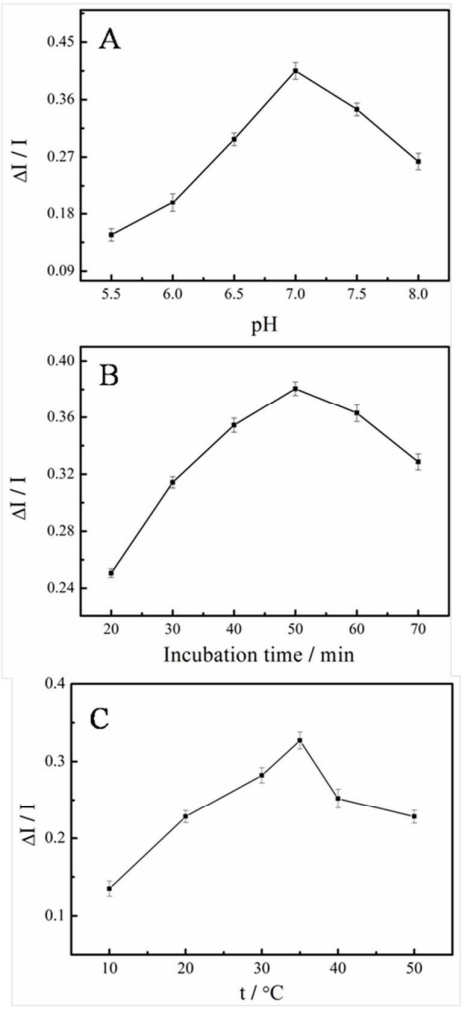

Fig. 7. Influence of the pH of the PBS (A), incubation time (B) and incubation temperature (C) on the current responses of the developed immunosensor.

The analytical performance of the immunoassay has been compared with those of other CEA immunoassays reported (Table 1). The comparative data suggested superiority of the present sensor over some earlier reported methods, especially the detection limit. The good electrochemical performance was ascribed to the large amount of AuNPs with an average diameter of about (10±2) nm, accordingly more anti-CEA can be absorbed on the electrode surface, and can enhance the access chance of the antigen and antibody. Besides, the good electrons transfer capability of AuNPs/PEDOT/GR can greatly enhance the electrochemical signal, so the immunosensor possessed higher sensitivity than previously works.

3.5 Selectivity, reproducibility and stability of the immunosensor

The selectivity of the proposed immunosensor plays an important role in analyzing biological samples without separation. α-Fetoprotein (AFP) was usually used to test the selectivity of the biosensor for CEA (the concentration of CEA is 0.4 ng mL^{-1}). AFP, like CEA, is one type of the tumor markers. The anti-CEA/AuNPs/PEDOT/GR/GCE blocked by BSA was separately exposed to 10 ng mL^{-1} of AFP and the current response was recorded. As can be seen in Fig. 9A, the decrease in the current of AFP was much lower than that of the CEA. In addition, the effects of glucose, dopamine, glycine and L-glutamate, which may exist in human serum, were also investigated. Results showed that higher current was observed with the 0.4 ng mL^{-1} of CEA than those of interfering substances. This suggested that the current response caused by the interaction of CEA and anti-CEA was specific without much interference from nonspecific adsorption of other interferents.

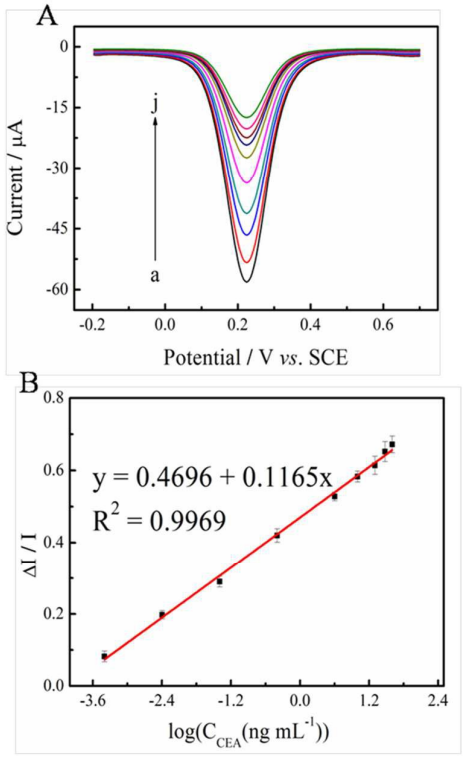

Fig. 8. Differential pulse voltammetry of the immunosensor after being incubated with different concentrations of CEA (a–j: 0, 0.0004, 0.004, 0.04, 0.4, 4, 10, 20, 30 and 40 ng mL^{-1}) (A). The calibration curve based on the change of the DPV peak currents versus the logarithm of the concentrations (B).

RSC Advances Accepted Manuscript

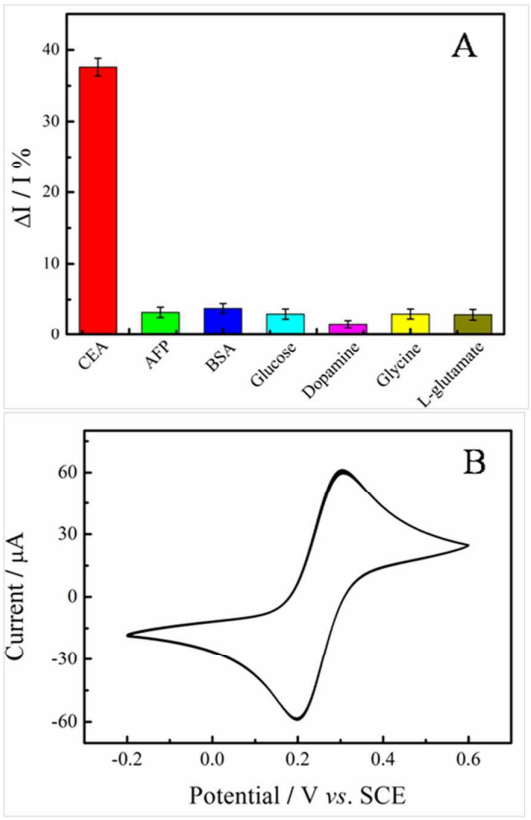

Fig. 9. (A) Comparison of the response of the immunosensor to 0.4 ng mL^{-1} CEA, 10 ng mL^{-1} AFP, BSA, glucose, dopamine, glycine and L-glutamate. (B) The stability of the immunosensor at successive cycle scan.

To evaluate the reproducibility of the immunosensor, a series of five different electrodes were prepared for the detection of 0.4 ng mL^{-1} CEA. DPV was used to record the electrochemical signal in 5.0 mM $[Fe(CN)_6]^{3-/4-}$ in 10 mM PBS solution (pH 7.0). The relative standard deviation (RSD) of the measurements for the five electrodes was 4.17%, which suggested that the reproducibility of the proposed immunosensor was quite good.

The stability of the immunosensor was also investigated by successive cycle scan and long-term storage assay. After 20 successive CV measurements under optimal conditions at a scan rate of 50 mV s^{-1}, a 5.23% decrease in the initial response was observed (Fig. 9B). The stability of the immunosensor was studied after storage at 4 °C for a 15-day period, the activity of immunosensors can maintained at 81.2%, demonstrating a good stability of the immunosensor.

3.6 Recovery and clinical application of the proposed immunosensor

The feasibility of the proposed method for the detection of CEA was evaluated by applying it to assay different concentrations of CEA added in human serum. Tests were performed by immersing the biosensor in five different concentrations of CEA respectively. The experimental results are shown in Table 2, and the recoveries are in the range from 97.00 to 103.20%, indicating that the immunosensor can be effectively applied to the determination of CEA in human serum.

4 Conclusions

In summary, a new electrochemical immunosensor was proposed by using AuNPs/PEDOT/GR nanocomposite material for detecting CEA. The significantly enhanced sensitivity relied on the good conductivity, large specific surface area and excellent biocompatibility of AuNPs/PEDOT/GR nanocomposite. Under optimized conditions, the immunosensor exhibited a wide linear range (0.0004 to 40 ng mL^{-1}), low detection limit (0.1 pg mL^{-1}), acceptable reproducibility, selectivity and stability. It was also successfully applied for the determination of CEA in human serum sample with good accuracy.

Table 1 Analytical performance of electrochemical immunosensors for detection of CEA.

Immunosensors	Linear range (ng·mL^{-1})	Detection limit (ng·mL^{-1})	References
3D-AuNPs/GN	0.001-10	0.00035	[9]
NGC-PWE[a]	0.001-10	0.0006	[43]
Chit-AuNPs/GCE	0.5-60	0.2	[44]
PTGO/GCE[b]	0.01-60	0.005	[45]
AuNPs/thionine/Nafion/GCE	0.01-12	0.005	[46]
AuNPs/L-cys/Nafion/CdS-GR/GCE	0.01-10.0	0.0038	[47]
AgNPs/DNA/thionine/SCPE	0.03-3	0.01	[48]
AuNPs/PEDOT/GR/GCE	0.0004-40	0.0001	This method

NGC-PWE[a]: nanoporous gold/chitosan modified paper working electrode;
PTGO/GCE[b]: platinum-thionine-graphene nanocomposite modified glassy carbon electrode.

RSC Advances Accepted Manuscript

Table 2 The recovery of the prepared immunosensor.

Sample	Added of CEA (ng mL^{-1})	Found (ng mL^{-1})	Recovery (%)
1	1.00	0.97	97.00
2	5.00	5.16	103.20
3	10.00	10.28	102.80
4	20.00	19.74	98.70
5	30.00	29.13	97.10

Acknowledgements

We are grateful to the National Natural Science Foundation of China (grant number: 51302117, 51303073, 51463008), Ganpo Outstanding Talents 555 projects (2013), the Training Plan for the Main Subject of Academic Leaders of Jiangxi Province (2011), the Natural Science Foundation of Jiangxi Province (grant number: 20151BAB203018, 20142BAB206028 and 20142BAB216029), Jiangxi Provincial Department of Education (GJJ11590, GJJ13258), Postdoctoral Science Foundation of China (2014M551857 and 2015T80688), Postdoctoral Science Foundation of Jiangxi Province (2014KY14) and the Science and Technology Landing Plan of Universities in Jiangxi province (KJLD12081) for their financial support of this work.

References

1 M. Grunnet, J. B. Sorensen, *Lung Cancer*, 2012, **76**, 138–143.
2 F. Y. Kong, M. T. Xu, J. J. Xu, H. Y. Chen, *Talanta*, 2011, **85**, 2620–2625.
3 H. Tang, J. H. Chen, L. H. Nie, Y. F. Kuang, S. Z. Yao, *Biosens. Bioelectron*., 2007, **22**, 1061–1067.
4 K. J. Huang, D. J. Niu, W. Z. Xie, W. Wang, *Anal Chim Acta*, 2010, **659**, 102–108.
5 B. B. Chen, B. Hu, P. Jiang, M. He, *Analyst*, 2011, **136**, 3934–3942.
6 J. P. Lia, H. L. Gao, Z. P. Chen, X. P. Wei, C. F. Yang, *Anal. Chim. Acta*, 2010, **665**, 98–104.
7 K. Kudoh, Y. Kikuchi, T. Kita, T. Tode, M. Takano, J. Hirata, Y. Mano, K. Yamamoto, I. Nagata, *Gynecol. Obstet. Invest*., 1999, **47**, 52–57.
8 M. J. A. Engelen, H. W. A. de Bruijn, H. Hollema, K. A. ten Hoor, P. H. B. Willemse, J. G. Aalders, A. G. J. van der Zee, *Gynecol. Oncol.*, 2000, **78**, 16–20.
9 G. Q. Sun, J. J. Lua, S.G. Ge, X. R. Song, J. H. Yu, M. Yan, J. D. Huang, *Anal. Chim. Acta*, 2013, **775**, 85–92.
10 K. J. Huang , J. Li, Y. M. Liu, X. Y. Cao, S. Yu, M. Yu, *Microchim. Acta*., 2012, **177**, 419–426.
11 B. Qu, X. Chu, G. Shen, R. Q. Yu, *Talanta*, 2008, **76**, 785–790.
12 W. Lei, W. Si, Y. Xu, Z. Gu, Q. Hao, *Microchim. Acta*., 2014, **181**, 707–722.
13 H. Pang, Y. C. Zhang, T. Chen, B. Q. Zeng, Z. M. Li, *Appl. Phys. Lett*., 2010, **96**, 251907.
14 K. S. Lee, Y. Lee, J. Y. Lee, J. H. Ahn, J. H. Park, *Chem. Sus. Chem*., 2012, **5**, 379–382.
15 L. B. Groenendaal, F. Jonas, D. Freitag, H. Pielartzik, J. R. Reynolds, *Adv. Mater*., 2000, **12**, 481–492.
16 F. Jonas, W. Krafft, B. Muys, *Macromol. Symp*., 1995, **100**, 169–173.
17 H. Mao, X. Liu, D. Chao, L. Cui, Y. Li, W. Zhang, C. Wang, *J. Mater. Chem*., 2010, **20**, 10277–10284.
18 F. Jiang, R. Yue, Y. Du, J. Xu, P. Yang, *Biosens. Bioelectron*., 2013, **44**, 127–131.
19 C. Bora, S. K. Dolui, *Polymer*, 2012, **53**, 923–932.
20 O. C. Compton, S. T. Nguyen, *Small*, 2010, **6**, 711–723.
21 Q. W. Chen, L. Y. Zhang, G. Chen, *Anal. Chem*., 2012, **84**, 171–178.
22 Y.S. Gao, L. P. Wu, K. X. Zhang, J. K. Xu, L. M. Lu, X. F. Zhu, *Chin. Chem. Lett*., 2015, **26**, 613–618.
23 Q. L. Hao, H. L. Wang, X. J. Yang, L. D. Lu, X. Wang, *Nano Res*., 2011, **4**, 323–333.
24 L. Li, G. Yan, J. Wu, X. Yu, Q. Guo, Z. Ma, Z. Huang, *J. Polym. Res*., 2009, **16**, 421–426.
25 X. Y. Li, Z. Yi , H. Tang , X. Chu, R. Q. Yu, *Anal. Methods*, 2014, **6**, 2221–2226.
26 L. Zhu, L. L. Xu, N. M. Jia, B. Z. Huang, L. Tan, S. F. Yang, S. Z. Yao, *Talanta*, 2013, **116**, 809–815.
27 K. X. Zhang, J. K. Xu, X. F. Zhu, L. M. Lu, X. M. Duan, *J. Electroanal. Chem*., 2015, **739**, 66–72.
28 X. W. Wang, Z. Zhang, X. L. Yan, Y. H. Qu, Y. Q. Lai, J. Li, *Electrochim. Acta*, 2015, **155**, 54–60.
29 Y. C. Si, E. T. Samuski, *Nano Lett*., 2008, **8**, 1679–1682.
30 S. Chen, J. Zhu, X. Wu, Q. Han, X. Wang, *ACS Nano*., 2010, **4**, 2822–2830.
31 C. Xu, X. Wang, J. Zhu, X. Yang, L. Lu, *J. Mater. Chem*., 2008, **18**, 5625–5629.
32 K. J. Huang, L. Wang, H. B. Wang, T. Gan, Y. Y. Wu, J. Li, Y. M. Liu, *Talanta*, 2013, 114, 43–48.
33 X. L. Ye, Y. L. Du, K. Y. Duan, D. B. Lu, C. M. Wang, X. Z. Shi, *Sens. Actuators B*., 2014, **203**, 271–281.
34 S. B. Yoon, K. B. Kim, *Electrochim. Acta*, 2013, **106**, 135–142.
35 T. Lindfors, Z. A. Boeva, R. M. Latonen, *RSC Adv*., 2014, **4**, 25279–25286.
36 W. M. Si, W. Lei, Z. Han, Q. L. Hao, Y. H. Zhang, M. Z. Xia, *Sens. Actuators B*., 2014, **199**, 154–160.
37 N. Hui, S. Wang, H. B. Xie, S. H. Xu, S. Y. Niu, X. Luo, *Sens. Actuators B*., 2015, **221**, 606–613.
38 K. J. Huang, L. Wang, Y. J. Liu, T. Gan, Y. M. Liu, L. L. Wang, Y. Fan, *Electrochim. Acta*, 2013, **107**, 379–387.
39 L. Zhang, R. Jamal, Q. Zhao, M. Wang, T. Abdiryim, *Nanoscale Res Lett*., 2015, **10**,148-152.
40 S. V. Selvaganesh, J. Mathiyarasu, K. L. N. Phani, V. Yegnaraman, *Nanoscale Res Lett*., 2007, **2**, 546–549.
41 K. J. Huang , J. Y. Sun, C. X. Xu, D. J. Niu, W. Z. Xie, *Microchim. Acta*., 2010, **168**, 51–58.
42 L. Li, C. Ma, Q. K. Kong, W. P. Li, Y. Zhang, S. G. Ge, M. Yan, J. H. Yu, *J. Mater. Chem. B*, 2014, **2**, 6669–6674.
43 L. Li, W. P. Li, C. Ma, H. M. Yang, S. G. Ge, J. H. Yu, *Sens. Actuators B*., 2014, **202**, 314–322.
44 X. Chen, X. L. Jia, J. M. Han, J. Ma, Z. F. Ma, *Biosens. Bioelectron*., 2013, **50**, 356–361.

RSC Advances Accepted Manuscript

This journal is © The Royal Society of Chemistry 20xx

45 B. Su, D. Tang, J. Tang, Y. Cui, G. Chen, *Biosens. Bioelectron*., 2011, **30**, 229–234.
46 Q. Li, D. Tang, J. Tang, B. Su, J. Huang, G. Chen, *Talanta*, 2011, **84**, 538–546.
47 G. F. Shi, J. T. Cao, J. J. Zhang, K. J. Huang, Y. M. Liu, Y. H. Chen, *Analyst*, 2014, **139**, 5827–5834.
48 W. Wu, P. Yi, P. He, T. Jing, K. Liao, K. Yang, H. Wang, *Anal. Chim. Acta*, 2010, **673**, 126–132.

RSC Advances Accepted Manuscript